RAL-93-091

Science and Engineering Research Council
Rutherford Appleton Laboratory
Chilton DIDCOT Oxon OX11 0QX

RAL-93-091

Double-Crystal Analyser System for the Prisma Spectrometer: Test of a Prototype

C Petrillo F Sacchetti M Hagen and U Steigenberger

November 1993

DOUBLE-CRYSTAL ANALYSER SYSTEM FOR THE PRISMA SPECTROMETER: TEST OF A PROTOTYPE

C. Petrillo and F. Sacchetti

Dipartimento di Fisica, Universita' di Perugia, Via Pascoli, 06100 Perugia, Italy

and

Istituto di Struttura della Materia del Consiglio Nazionale delle Ricerche, Via E. Fermi 38, 00044 Frascati, Italy

M. Hagen et al.

Department of Physics, Keele University, Keele, Staffordshire ST5 5BG, U.K.

and

ISIS Science Division, Rutherford Appleton Laboratory, Chilton, Didcot, Oxon. OX11 0QX, U.K.

U. Steigenberger

ISIS Science Division, Rutherford Appleton Laboratory, Chilton, Didcot, Oxon. OX11 0QX, U.K.

Abstract

A prototype of a double-analyser system has been tested at the ISIS pulsed neutron source in order to determine the performance of such an analysing device in the low energy transfer region. The performance of such a system has been found satisfactory in terms of reflectivity and energy resolution as well as alignment procedures. Based on our test results we propose the construction of a second arm for the PRISMA spectrometer at ISIS. This new arm would enable us to perform measurements with much improved energy resolution and to extend the wavevector transfer range to much smaller values thus improving the instrument performance significantly for magnetic scattering experiments. The new, modular approach of the upgrade will also strengthen the flexibility of the instrument and open up the opportunity for further instrumental developments, for example the introduction of a polarization option.

I. Introduction

The multi-analyser spectrometer **PRISMA** (**PR**ogetto dell'**I**stituto di **S**truttura della **MA**teria del CNR) designed and constructed under the international collaboration between the Italian Consiglio Nazionale delle Ricerche (CNR) and the British Science and Engineering Research Council (SERC) and installed and commissioned at the Spallation Neutron Source ISIS, Rutherford Appleton Laboratory U.K., has now been working for four years[1,2]. During this period, several modifications and improvements to the original design have been made, such as the installation of a disc chopper in the incident beam in order to reduce the background and the insertion of sixteen high reflectivity pyrolitic graphite analysers in order to increase the measured intensity.

The general performance parameters of such an instrument are described in Refs. 2 and 3 and the results of some of the most recent scattering experiments performed on PRISMA are reported in Refs. 4-9. From these papers it can be seen that one of the advantages of the PRISMA spectrometer is in performing overview measurements of the phonon response function along high symmetry directions extending over a wide energy transfer range. The simultaneous investigation of extended portions of the momentum-energy space, made possible by the time of flight nature of the spectrometer, allows an easy identification of possible interesting features even if their location

in the Brillouin zone is not known *a priori*. Furthermore the inspection of a wide energy range around one-phonon peaks is important when studying the energy dependence of the phonon self-energy and is particularly relevant when considering the electron-phonon interaction in systems which are undergoing a transition, such as a structural phase transition or a superconducting transition. In such cases another advantage of PRISMA shows up: the measurement of the inelastic spectrum as a function of some external parameter, such as temperature or magnetic field, can be performed while maintaining the sample in the same fixed position and without any change of the spectrometer setting. In such a way, the risk of possible instrumental misalignements or mechanical vibrations during the repositioning of both sample and spectrometer is avoided.

A major limitation of the present version of PRISMA comes from the intrinsic mechanical constraints on the detector arms. Avoiding possible collisions between the detector arms imposes an additional constraint, other than the kinematic one, to the ranges of energy and momentum transfer possible on PRISMA. In particular, the maximum Bragg angle $2\theta_A$ attainable at the analyser crystals is 37°, which results in a minimum final energy E_f of the order of 20 meV for the PG(002) analyser crystals. This limitation on the minimum value of E_f does not allow measurements with high energy resolution at low energy transfers. As reported in Ref. 3, the relative energy resolution $\Delta E/E_f$ is roughly constant over the range 20 meV < E_f < 60 meV, as deduced

from measurements on a vanadium standard. Hence, high E_f values correspond to large values of ΔE. Such a behaviour is dramatic when measuring acoustic phonon peaks at low energy transfers since, in some cases, the resolution is not sufficient to distinguish between the different branches. Another consequence of the high value of the *minimum* E_f is reflected in the accessible range of the momentum transfer Q. The resulting values of Q_{min} are relatively high and this sets a serious limitation to the study of magnetic excitations where the form factor is a strongly decreasing function of Q.

These limitations could be overcome by use of a double- crystal analyser system especially designed for covering the low energy and momentum transfer range with good energy resolution. Such a double-crystal analyser system, having a large range of rotation for both crystals would not require any movement of the detector when E_f is changed, hence solving the clashing problem. In this report, the operating principles of a double-crystal analyser will be briefly summarized. An extensive description of the mechanical prototype will be given together with a discussion of the neutron test measurements performed at ISIS. Finally the conceptual design, suggested by the results of these measurements, of a multi-double-crystal analyser arm to be installed on PRISMA will be presented. The mechanical design of such a system has been developed for fitting onto the present main body of the PRISMA spectrometer and for operating alternatively to the present sixteen-analyser arm.

II. Double-crystal analyser system

The operating principles of the double-crystal system have been extensively described in several textbooks and papers[10,11], mainly as an optical device for X-ray sources. Typically two possible settings of the two perfect crystals are employed, denoted by (m,n) and (m,-n), m and n being respectively the m-th order of reflection from the first crystal and the n-th order of reflection from the second crystal. The two arrangements are shown in Fig.1 when m and n are equal, i.e. the reflection takes place off the same order from each crystal. The (1,-1) setting is normally referred to as the *parallel* or *non-dispersive* arrangement, while the (1,1) setting is called the *anti-parallel* or *dispersive* arrangement. The optical properties of the two settings are quite different. In the two-crystal diffraction experiment, the first crystal is generally fixed in Bragg reflection while the second crystal (the sample) is scanned through the Bragg position. The (1,-1) non-dispersive setting yields a reciprocal space focusing and it has the important property of giving the same reflection curve for all the incoming wavelengths (closely neighbouring), provided that the reflection curve of the first crystal can be assumed to be independent of the wavelength[10]. On the other hand, in the (1,1) anti-parallel setting, wavelength components are dispersed at the second crystal and this is an appropriate method of studying the wavelength dispersion.

For the present purposes, the (1,-1) arrangement is adopted and, even though both crystals are free to rotate, they are operated in a fixed relation during the measurement, once the initial alignment has been performed. The double-crystal system is used to select a given final energy and the energy transfer is scanned by the white spectrum of the incoming beam. It should be noted that, contrary to the ideal double-crystal system for X-ray diffraction experiments, both the crystals are far from ideally perfect. Crystals with quite a large mosaic spread have to be employed in order to get an integrated intensity which is as high as possible.

The same kind of scans possible on the current PRISMA can be performed using the double-crystal system and the kinematic equations for $(Q,h\omega)$ scans corresponding to inelastic measurements are exactly the same[1,2]. As discussed in Ref. 2, the lowest *reasonable* limit (in principle $-E_f$) to the exchanged energy should be significantly larger than $E_\perp$, where:

$$E_\perp = -\frac{\hbar^2 Q_\perp^2}{2m} \qquad \text{and}$$

$$Q_\perp = k_f \sin\Phi = \frac{\pi \sin\Phi}{d_A \sin\theta_A} \qquad Q_\parallel = k_0 - k_f \cos\Phi$$

k_f and k_0 are the wavevectors of the final and incoming neutrons, Φ and θ_A the scattering angle and the Bragg angle at the analyser and d_A the analyser lattice spacing.

The upper and lower limits of k_f, and hence of E_f, are determined for a given d_A (fixed reflecting plane of a chosen analyser) by the rotation range for the analyser Bragg angle θ_A, which is the same for both of the crystals in (1,-1) setting, and by the maximum translation possible for the second crystal. The reference configuration for the two crystals is shown in Fig. 2: the origin of the translation of the second crystal is assumed when the Bragg angle θ_A is equal to 45° for both the crystals. The final energy E_f can be changed by rotating both crystals by the same amount and simultaneously translating the second crystal by the distance:

$$T = L \text{ cotg } (2\theta_A)$$

where L is the reference distance between the analysers, as shown in Fig.2.

The value of the minimum angle at the analysers is therefore defined by the maximum translation possible for the second crystal, having fixed the distance L. In particular, the translation range is mechanically limited by the available space between the analyser and detector which, in the present configuration of PRISMA, is fixed at 150 mm. The upper limit of the final energy E_f is consequently constrained while the minimum value of E_f, assuming for θ_A the nominal maximum limit equal to 45°, is defined only by the lattice spacing of the crystals.

In principle no limitation is set over the distance L between the crystals even though the test measurements performed on the prototype

system and described in the following suggest a working configuration with the two crystals as close as possible. This choice allows for an easier alignment because of the high collimation of the beam emerging from the first crystal and prevents absorption and scattering of neutrons by the air along the path. On the other hand, too small a distance between the crystals can produce spurious peaks in the detected spectrum if the second crystal is directely illuminated by the incoming beam (which has a finite width).

In Figs. 3a and 3b the final energy and Bragg angle θ_A at the analyser are shown as function of both translation T and the distance L. Calculations have been performed for the case of the (002) reflecting plane of pyrolitic graphite (d=3.355 Å). The choice T_{max}=150 mm and L=100 mm, which sounds quite reasonable in view of the present considerations, yields:

$$16.8° < \theta_A < 45° \qquad 3.63 \text{ meV} < E_f < 21.7 \text{ meV}$$

The final energy is thus covering the range required for an improvement of the present PRISMA spectrometer.

Finally, in Fig. 4 the maximum and minimum energy transfer obtainable with the double-graphite-analyser system is shown against the momentum transfer and compared to that of a single arm on PRISMA.

III. Mechanical prototype and neutron test measurements

In order to check the operation of the double-crystal option for an analyser system on an indirect geometry neutron spectrometer, a simple mechanical prototype has been designed and built at the Istituto di Struttura della Materia del CNR. The prototype has been installed and commissioned at ISIS and test measurements have been performed using the incoming neutron beam of the TEB beam line.

The angular rotation of the two crystals was carried out using stepper motors (Micro-Controle UE 30 PP 10000) with a step size of 0.018° in the half-step mode. The second crystal was fixed to a translation table (Micro-Controle UT 100) which could be stepped in units of 1 μm. The total translation range 75 mm. For the test measurements two types of double-analyser system have been considered: two slab shaped pyrolitic graphite crystals (50mm x 60mm) with a mosaic spread of 0.5° of the type currently installed on PRISMA and a mixed system of one pyrolitic graphite slab as the first crystal and a disk shaped squashed germanium crystal ((110) face, 15mm thickness, 50mm diameter) having a mosaic spread of the order of 0.3° as the second crystal. In this case the (002) Bragg reflection (d_A=3.355 Å) was selected as the analysing plane from the graphite crystals, while the (111) Bragg plane (d_A=3.326 Å) was selected for the germanium, thus having a good match for the d-spacings of the two crystals. The double-graphite system was operated in reflection geometry, whereas in

the mixed graphite-germanium system, the germanium crystal was mounted in transmission geometry. This configuration was dictated by the need to match the lattice spacings of the two crystals and a (111) cut germanium crystal was not available. Specially designed supports for the crystals, directly connected to the rotation axes of the motors, were used.

Three closely set ^{3}He proportional detectors at 20 atm pressure, operating at 2 kV, 10 mm in diameter with a 60 mm active length, were used in a vertical configuration.

Two sets of Soller collimators 350 mm long with horizontal divergences of 60′ and 40′ were used to check collimation effects on the line shape of the scattered intensity. They were mounted on the arm between the sample and the first crystal and on the arm between the second crystal and the detectors. Because of the size of these collimators, no measurements were performed for the case of mounting one of them in-between the two crystals.

An aluminium table (thickness 15mm, size 500mm x 1000mm) carrying the analysers, collimators and detectors was fixed on a moveable Φ arm. The absolute determination of the Φ angle was done by measuring the time of flight spectrum from a standard Ni powder, without any analyser in place.

The control of the stepper motors for rotation and translation was carried out using a driving system designed and constructed at the Istituto di Struttura della Materia, similar to that installed on

PRISMA. The data acquisition system was the standard ISIS DAE in normal use on TEB.

The relevant parameters for the prototype and for the analysers are given in Table I.

An initial check on the operation of the double-analyser system was performed by measuring the rocking curves[12,13] of each of the crystals individually, leaving one crystal fixed while rotating the other about a vertical axis. These measurements were performed using a monochromatic beam produced by Bragg reflection from a single crystal sample (lead (200) at Φ=90°). In Fig. 5 the intensity integrated over the time of flight spectrum at each point (1000μs<t<14000μs) is shown as function of the rotation angle, for both of the two pyrolitic graphite crystals.

The principal aims of these test measurements can be summarised as follows:

1- testing the resolution and intensity of low energy phonon peaks in a well known standard single crystal

2 - testing the resolution and intensity of the elastic peak from an incoherent scatterer as a function of the final energy E_f selected by the analyser system

3- testing the effects of the horizontal collimation on both the inelastic and elastic peaks.

These points have been examined for both the graphite-graphite and graphite-germanium double analyser systems. For comparison, the

measurements of both elastic and inelastic spectra have been repeated using a single graphite crystal as the analyser.

IIIa. Inelastic scattering measurements

The phonon response function was measured using a single crystal of lead of cylindrical shape, 2.5 cm in diameter and 5 cm in height, and a vertical axis parallel to the [001] direction. This sample was the same as that used in a previous experiment on the PRISMA[4] spectrometer. The final energy selected by the analyser, 6.7 meV, was chosen in order to have the scan direction along the [110] direction passing through the (200) reciprocal lattice point. The incoming beam direction is therefore along the [110] direction, as shown in Fig.6. The scattering angle Φ was fixed at 81.7°. Fig.7 shows the inelastic spectrum using a) the graphite-graphite system without any collimation, b) with a collimation of 60′ between sample and the first analyser, c) with the mixed analyser system and d) using a single graphite crystal. In the two latter cases, a 60′ collimator was in place between the sample and the first analyser. The data presented in Fig.7 have been obtained by correcting the time of flight spectrum for the flux distribution of the incoming beam, subtracting a time independent background and transforming the data into energy transfer units. From Fig.7 some effects can be seen immediately: because of the negligible incoherent cross section of lead, the elastic peak has to

be attributed to some Bragg peak process, not necessarly from the sample. It is filtered out by the insertion of the collimator. It is again present when the second crystal is germanium, and the collimator is mounted, probably because of the large size of the germanium crystal.

The solid lines shown in Fig.7 are fits to the inelastic peaks obtained using the simple model function:

$$I(\omega) = [n(\omega) + 1] \quad \frac{\gamma\ \omega}{(\omega - \omega_o)^2 + (\gamma\ \omega)^2}$$

where $n(\omega)$ is the Bose factor and γ and ω_o are left as free parameters. This function takes into account the relevant features of the scattered intensity and fits well the data also in the tails of the phonon groups. From these fits, energy positions ω_o and Full Width at Half Maximum (FWHM) $2\gamma\omega_o$ of the phonon peaks can be deduced. In Table II the FWHM values and the integrated intensities under the peaks are summarized for all the different configurations. The effect of a 60′ horizontal collimation on the estimated widths and integrated intensities of the phonon peaks appears to be negligible at least at the level of accuracy of the present test experiment. The insertion of the second crystal causes a loss of integrated intensity of the order of 40% in comparison with the single-analyser configuration. A final remark is deserved for the mixed graphite-germanium system: apparently

with this choice the two phonon peaks are not well resolved and the significant decrease in the integrated intensity is partly due to the narrow mosaic spread of the germanium crystal.

The two peaks occurring at phonon energies and wavevectors equal to (0.73meV, 0.16Å^{-1}) and (1.32meV, 0.09Å^{-1}) can be identified as transverse $T_1[\zeta\zeta 0]$ and longitudinal $L[\zeta\zeta 0]$ acoustic phonons respectively, the $T_2[\zeta\zeta 0]$ branch is not contributing in the present configuration since the polarization vector is perpendicular to the momentum transfer. In Fig.8 our data of the low energy L and T_1 branches along the [110] direction are compared to those from Ref.14. This comparison is quite satisfactory and the figure clearly demonstrates the ability of the double-crystal setting to cover the low energy regions with a very good resolution.

IIIb. Elastic scattering results

The overall trend in the resolution of the double-analyser system can be deduced from the measurements of the width of the elastic line from an incoherent scatterer as a function of the analyser energy[2,3]. Elastic line profiles from a perspex sample (10x20x50 mm^3) have been collected using the double-graphite system at three different values of final energy, 4.8 meV, 6.7 meV and 9 meV (PG (002), fixed scattering angle Φ=81.7°). In order to get an estimate of the decrease

in intensity due to the use of two crystals, the same measurements have been repeated with a single graphite analyser in place.

The time-of-flight spectra also contain the elastic line due to the reflection from the graphite (004) planes, corresponding respectively to the final energies 19.2 meV, 26.8 meV and 36 meV. In principle, the width of these peaks can also be studied in order to get the general trend over a wider range of final energies. The effect of the collimation on the incoherent elastic scattering from perspex was investigated by separately inserting either a 60′ collimator or a 40′ collimator between the sample and the first analyser. In addition a spectrum from the vanadium sample was collected at 4.8 meV final energy from the (002) planes with a 40′ collimator in place.

Fig.9a shows the elastic spectra from perspex measured using the (002) reflection plane of the double-analyser system without any collimation, with 60′ collimation and with 40′ collimation. Corresponding results for E_f=19.2 meV final energy are shown in Fig.9b. In comparison Fig.10 shows the results obtained with single graphite analyser at E_f=4.8 meV, 6.7 meV and 9 meV using a 60′ collimator. In Fig. 11 the spectrum measured with the vanadium standard is shown. Table III summarizes the results of the FWHM of the peaks, obtained by Gaussian fits.

In order to extract some quantitative information about the energy resolution from the data presented in Figs.9-11, we compare all the data to those of the (002) double-analyser. The data from (004) are

affected by a greater uncertainty. In Fig.12 the variation of the width of the elastic line, as measured by the double-analyser system, versus the (002) analyser energy is shown for all of the different collimation configurations. From this figure and from the data reported in Table III it can be seen that the dependence of ΔE on the final energy E_f is linear within good approximation over the range 4.8 meV < E_f < 10meV.

The experimental ratio $\Delta E/E_f$ in perspex is dominated by the Bragg angle and mosaic spread distribution of the analysers. The effect on the energy resolution due to the collimation is noticeable whereas the width of the incoming neutron pulse plays only a small role. A qualitative estimate of the various contributions to the resolution can be obtained by assuming that all the distribution functions are represented by Gaussians and that the widths of the distributions are approximated by the FWHM of the Gaussians. With this assumption the resulting wavelength distribution $\Delta\lambda$ is given by:

$$(\Delta\lambda)^2 = (\Delta\lambda_o)^2 + (\Delta\lambda_a)^2$$

where $\Delta\lambda_o$ is the width of the incoming neutron pulse and $\Delta\lambda_a$ is the width due to both the mosaic distribution of the analysers and the collimations. In the double crystal setting $\Delta\lambda_a/\lambda_a$ can be written as:

$$\Delta\lambda_a/\lambda_a = \sqrt{2}\ \Delta\theta_{eff}\ \mathrm{cotg}(\theta_A)$$

where $\Delta\theta_{eff}$ is the convolution of the angular distribution of the beam in the scattering plane with the distribution of the mosaic structure

and θ_A, the Bragg angle, is equal for the two analysers. Since $\Delta E/E = 2\Delta\lambda/\lambda$, one gets:

$$(\Delta E/E)^2 = 4\ (\Delta\lambda_o/\lambda_o)^2 + 8\ [\Delta\theta_{eff}\ \mathrm{cotg}(\theta_A)]^2$$

In Fig. 13 the experimental determined ratio $(\Delta E/E)^2$ is shown as a function of $[\mathrm{cotg}(\theta_A)]^2$. Considering that when $\mathrm{cotg}(\theta_A)=0$ the only contribution to $\Delta E/E$ comes from the pulse width $\Delta\lambda_o/\lambda_o$, which can be assumed to be constant over a narrow wavelength range, the extrapolation of the experimental ratios to zero allows the $\Delta\lambda_o/\lambda_o$ contribution to be deduced. Subtraction of $4(\Delta\lambda_o/\lambda_o)^2$ from the experimental ratio $(\Delta E/E)^2$ yields the *experimental* widths $\Delta\theta_{eff}$, which can be used in order to estimate the calculated ratio $(\Delta E/E)_{cal} = 2\sqrt{2}\ \Delta\theta_{eff}\ \mathrm{cotg}(\theta_A)$. In Table IV a comparison between calculated and experimental ratios is reported together with the estimate of $\Delta E/E$ which was obtained by neglecting the effects of both collimation and incoming neutron pulse and using the nominal value of 0.5° for the mosaic spread of graphite crystals.

As a final remark, one can observe that the integrated intensity increases by nearly a factor of two going from the double-crystal to the single-crystal configuration. From Table III the resolution obtained with a single analyser appears to be worse than that found for the double-analyser. This is probably due to the absence of any collimation between analyser and counter.

The mechanical design of the double-analyser arm for the PRISMA spectrometer

Based on the results from our test measurements of the double analyser prototype, we propose to build a second scattering arm for the PRISMA spectrometer which will operate alternatively with the present scattering arm. The new scattering arm will consist of 5 analyser-detector arms. Each analyser-detector arm will have two graphite analyser crystals, 5 x 5 cm^2 in size, operating in double diffraction geometry. Both analyser crystals will be mounted on rotation tables allowing ±180° rotation; the second analyser will have additionally a translation stage in order to maintain the double diffraction geometry when changing E_f. The analyser energy range is determined by the relative position of the translation and the distance between the two analyser crystals, L. If we define the translation T for θ_A=45° (corresponding to E_f=3.63 meV for PG(002)) to be zero, then we find that for L=4.5cm we require for E_f=14meV a translation of T=52mm. If we take this as E_f^{max} then another 40mm of translation will allow us to reach an E_f^{min}=2.25 meV. Thus the total analyser transfer range is from 2.25 meV to 14 meV. The required total translation range of 77mm is commercially available as a small sized unit.

The distance L=45mm between the crystals has been chosen such to optimize the energy transfer range and to avoid at the same time self-

shielding of the crystals. The width of the neutron beam scattered from the sample and the projected width of the analyser crystals (45mm for E_f=2.25cm and 18mm for E_f=14meV) also agree with this choice.

The minimum distance from the sample to the first analyser (L_{A1}) and from the second analyser (L_{A2}) to the detector is determined by the requirement of collimators before and after the analysers. A minimum length of 12cm is required to allow reasonable collimation. We also need space in front of the first analyser for a vertical collimator. We estimate that L_{A1} should be 60cm and L_{A2} 20cm. The collimators will have an effective width of 30mm, corresponding to the beam width.

The individual arms should be arranged as close as possible. With the dimensions discussed above, this leads to an angular separation of 10°. As the separation in momentum transfer is much smaller for the double-analyser configuration due to the reduced analyser energies, this larger angular separation does not represent a problem. If a finer coverage in (Q,ω) space is required, then interleaving runs can be used. In order to facilitate the alignement of the analysers and the translation, we propose to introduce a hardware limit stop which, once calibrated, will serve as a reference point.

A table carrying the double-analyser assemble will be housed in a tight fitting shielding tank and the whole assembly will move when the scattering angle from the sample has to be changed. The shielding tank will be constructed in such a way that a change of configuration from the **new high resolution arm** to the **present high intensity arm** can be

accomplished easily between ISIS cycles. This modular approach will also enable us to develop and install in future other arms and thus enhance the capabilities of the instrument even further.

PRISMA has already demonstrated its potential to be an extremely versatile instrument, suited not only to the studies of single crystal excitations over a wide energy transfer range, but also suitable for e.g. critical or diffuse scattering experiments, single crystal diffraction experiments with high Q-resolution and very low background and more. The proposed upgrade will strengthen the role of PRISMA even further and a large part of the neutron scattering community will benefit from it.

Aknowledgments

We are grateful to the Institut Laue Langevin for providing us with a set of Soller collimators for these test measurements.

References

1- C. Andreani, C.J. Carlile, F. Cilloco, C. Petrillo, F. Sacchetti, Nuclear. Instrum. and Methods **A254**, 333 (1987).

2- U. Steigenberger, M. Hagen, R. Caciuffo, C. Petrillo, F. Cilloco and F. Sacchetti, Nuclear Instrum. and Methods B53, **87** (1991).

3- M. Hagen and U. Steigenberger, Nuclear Instrum. and Methods, **B72**, 239 (1992).

4- F. Sacchetti, R. Caciuffo, C. Petrillo and U. Steigenberger, J. Phys.: Condens. Matter **3**, 8759 (1991).

5- F. Sacchetti, O. Moze and C. Petrillo, Solid St. Commun. **81**, 195 (1992).

6- G. Chiarotti, C. Petrillo and A. Scacco, Physica B **180&181**, 312 (1992).

7- M. Hagen, M.T. Dove, M.J. Harris, U. Steigenberger and B.M. Powell, Physica B **180&181**, 276 (1992).

8- S. Tomiyoshi, T. Kaneko, U. Steigenberger, A.J. Chappell, M. Hagen and Y. Todate, Physica B **180&181**, 227 (1992).

9- M.T. Dove, M. Hagen, M.J. Harris, B.M. Powell, U. Steigenberger and B. Winkler, J. Phys. C **4**, 2761 (1992).

10- R.W. James, *The Optical Principles of the Diffraction of X-Rays*, (Bell & Sons LTD, London, 1958).

11- A.K. Freund, *X-Ray Optics for Synchrotron Radiation*, Proceedings of Brookhaven Biology Symposium, 1988.

12- B. Dorner and A. Kollmar, J. Appl. Cryst. **7**, 38 (1974).

13- B. Dorner, J. Appl. Cryst. **4**, 185 (1971).

14- B.N. Brockhouse, T. Arase, G. Caglioti, K.R. Rao and A.D.B. Woods, Phys. Rev. **128**, 1099 (1962).

Figure Captions

Fig. 1 - The two types of setting for the double-crystal system. a) the (1,1) arrangement; b) the (1 -1) arrangement.

Fig. 2 - Reference configuration for the (1 -1) setting of the double-crystal system.

Fig. 3 - a) Final energy E_f and b) Bragg angle at the analyser as a function of the translation T at the second analyser and the distance L between the two analysers.

Fig. 4 - Curves of the maximum and minimum energy transfers on the double-graphite system (solid lines) and on the PRISMA spectrometer (dashed lines) as a function of the momentum transfer.

Fig. 5 - Rocking curve of the (002) reflection from the double-graphite system. a) First analyser rocking, second analyser fixed; b) first analyser fixed, second analyser rocking.

Fig. 6 - Scan geometry superimposed on the Brillouin zone of lead.

Fig. 7 - Intensity versus energy (dots) as measured in lead using the double-graphite system with 60′ collimation (top left panel); the double-graphite system without any collimation (bottom left panel); a single graphite analyser with 60′ collimation (top right panel); the mixed graphite-germanium system with 60′ collimation (bottom right panel). The solid lines are fits to the peaks (see text).

Fig. 8 - Low-energy longitudinal (L) and transverse (T_1) phonon branches in lead along the [110] direction. Present data (dots); data from Ref. 14 (circles). The full lines are guides for the eye.

Fig. 9a - Elastic spectra from perspex measured using the (002) reflection plane from the double-graphite system at the three final energies 4.8meV (squares), 6.7meV (circles) and 9meV (dots). No collimation (left panel), 60′

collimation (central panel), 40′ collimation (left panel).
The full lines are gaussian fits to the peaks.

Fig. 9b - Elastic spectra from perspex measured using the (004) reflection plane from the double-graphite system at 19.2meV final energy. No collimation (left panel); 60′ collimation (central panel); 40′ collimation (right panel).
The full lines are gaussian fits to the peaks.

Fig. 10 - Elastic spectra from perspex measured using the (002) reflection plane (left panel) and the (004) reflection plane (right panel) from a single graphite analyser at three values of final energy (9 and 36meV: dots; 6.7 and 26.8meV: circles; 4.8 and 19.2meV: squares). In both the cases a 60′ collimation was used.
The full lines are gaussian fits to the data.

Fig. 11 - Elastic spectra from vanadium measured using the (002) reflection plane (left panel) and the (004) reflection plane (right panel) from the double-graphite system at one value of final energy (4.8 and 19.2meV respectively). In both the cases a 40′ collimation was used.
The full lines are gaussian fits to the data.

Fig. 12 - Full width at half maximum of the elastic line from perspex as a function of the (002) analyser energy. Data collected using the double-graphite system without any collimation (dots); with a 60′ collimation (circles) and with a 40′ collimation (squares). Lines are a guide for the eye.

Fig. 13 - Experimental ratio $(\Delta E/E)^2$ versus $(\mathrm{cotg}\theta_A)^2$ measured in perspex using the double-graphite system without any collimation (dots) with a 60′ collimation (circles) and with a 40′ collimation (squares). Lines are a guide for the eye.

Table Captions

Table I - Parameters for the prototype and the analysers.

Table IIa - Energy positions and widths of the $T_1[\zeta\zeta 0]$ and $L[\zeta\zeta 0]$ phonon branches in lead as measured by varying the analyser configuration.

Table IIb - Ratio of the integrated intensity of the transverse and longitudinal phonon peaks. The ratio is taken with reference to the single graphite analyser. The integrals are calculated using the fitted functions.

C-C: double-graphite system without any collimation;
C-C 60′: double-graphite system with 60′ collimation;
C 60′: single analyser of graphite with 60′ collimation;
C-Ge 60′: mixed graphite-germanium double-analyser with 60′ collimation.

Table IIIa - Full width at half maximum (FWHM) of the elastic line measured in perspex at three different final energies from double and single graphite analyser and with varying collimation. Data refer to both the (002) and the (004) reflection planes.

Table IIIb - Full width at half maximum (FWHM) of the elastic line from vanadium measured using the double-graphite system.

Table IV - Comparison between calculated and experimental $\Delta E/E$ ratios in perspex (see text). Data refer to the measurements using the (002) reflection plane from the double-graphite system and for different collimations.

Beam line	S9
Moderator	100K CH_4
Scattering angle Φ	81.7°
Distances	
Moderator-Sample	12.6 m
Sample-First Analyser	0.73 m
First Analyser-Second Analyser	0.086m
Second Analyser-Detector	0.15 m
Analyser Parameters	
Pyrolitic Graphite	50mm x 60mm
Nominal mosaic spread	0.5°
Lattice spacing	$d_{(002)}$=3.355Å
Germanium	50mm diameter 15mm thickness
Nominal mosaic spread	0.3°
Lattice spacing	$d_{(111)}$=3.266Å
Analyser Bragg angle	
C-C	38°; 31.38°; 26.7°
C-Ge	38°-39.2°; 31.38°-32.34°; 26.7°-27.49°
Final Energy	
from C-C (002)	4.8meV; 6.7meV; 9 meV
from C-C (004)	19.2meV; 26.8meV; 36meV
Translation at the second analyser	21.44mm; 44.27mm ; 63.87mm
Detectors	3 ^{3}He counters 60mm active length

Table I

		T_1		L	
		$\hbar\omega$(meV)	FWHM	$\hbar\omega$(meV)	FWHM(meV)
C-C		0.774±0.002	0.311±0.006	1.390±0.011	0.312±0.023
C-C	60'	0.711±0.004	0.329±0.013	1.330±0.011	0.369±0.028
C	60'	0.707±0.002	0.222±0.004	1.253±0.005	0.419±0.016
C-Ge	60'	0.807±0.006	0.367±0.016	1.369±0.037	0.80±0.17

Table IIa

		R_{T1}	R_L
C-C		0.657±0.011	0.369±0.019
C-C	60'	0.455±0.010	0.528±0.026
C	60'	1	1
C-Ge	60'	0.267±0.008	0.158±0.013

Table IIb

		(002)			(004)	
E_f(meV)		C-C	C	E_f(meV)	C-C	C
9		0.630±0.027		36		
6.7	No	0.411±0.036		26.8		
4.8		0.244±0.038		19.2	0.824±0.101	
9		0.478±0.048	0.633±0.032	36		3.056±0.104
6.7	60′	0.362±0.045	0.442±0.042	26.8		1.532±0.098
4.8		0.202±0.034	0.284±0.060	19.2	0.637±0.082	0.889±0.089
9		0.458±0.057		36		
6.7	40′	0.268±0.054		26.8		
4.8		0.213±0.065		19.2	0.527±0.182	

Table IIIa

		(002)		(004)
		C-C		C-C
E_f(meV)			E_f(meV)	
4.8	40′	0.162±0.047	19.2	0.515±0.057

Table IIIb

θ_B (deg)	E_f (meV)		$(\Delta\theta)_{eff}$ (deg)	$(\Delta E/E)_{exp}$	$(\Delta E/E)_{cal}$	$(\Delta E/E)_{crystal}$
26.7	9		0.64	0.070	0.063	0.049
31.38	6.7	**No**	0.65	0.061	0.053	0.040
38	4.8		0.65	0.051	0.041	0.032
26.7	9		0.45	0.053	0.044	0.049
31.38	6.7	**60'**	0.55	0.054	0.045	0.040
38	4.8		0.48	0.042	0.030	0.032
26.7	9		0.42	0.051	0.041	0.049
31.38	6.7	**40'**	0.33	0.040	0.026	0.040
38	4.8		0.39	0.044	0.025	0.032

Table IV

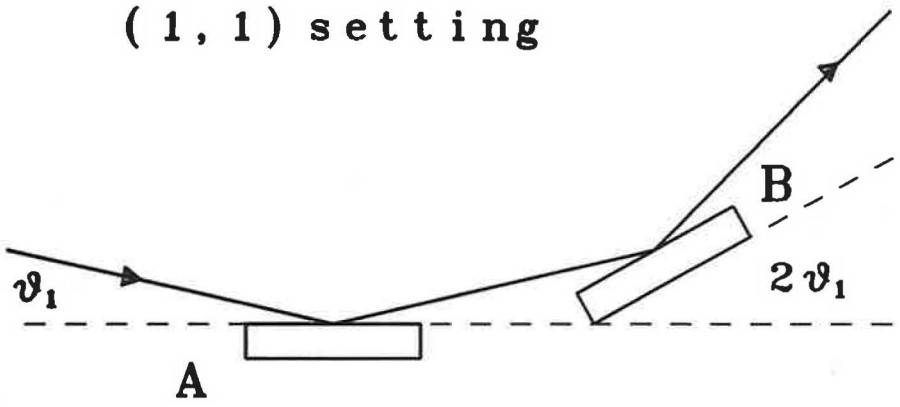

Fig. 1a

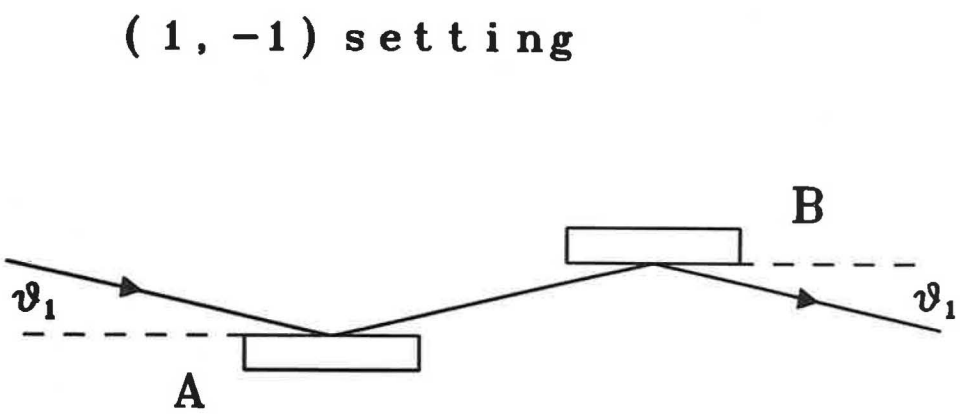

Fig. 1b

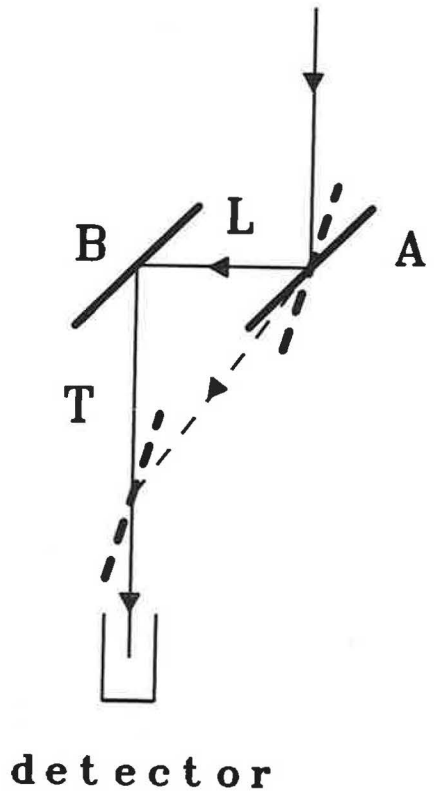

Fig. 2

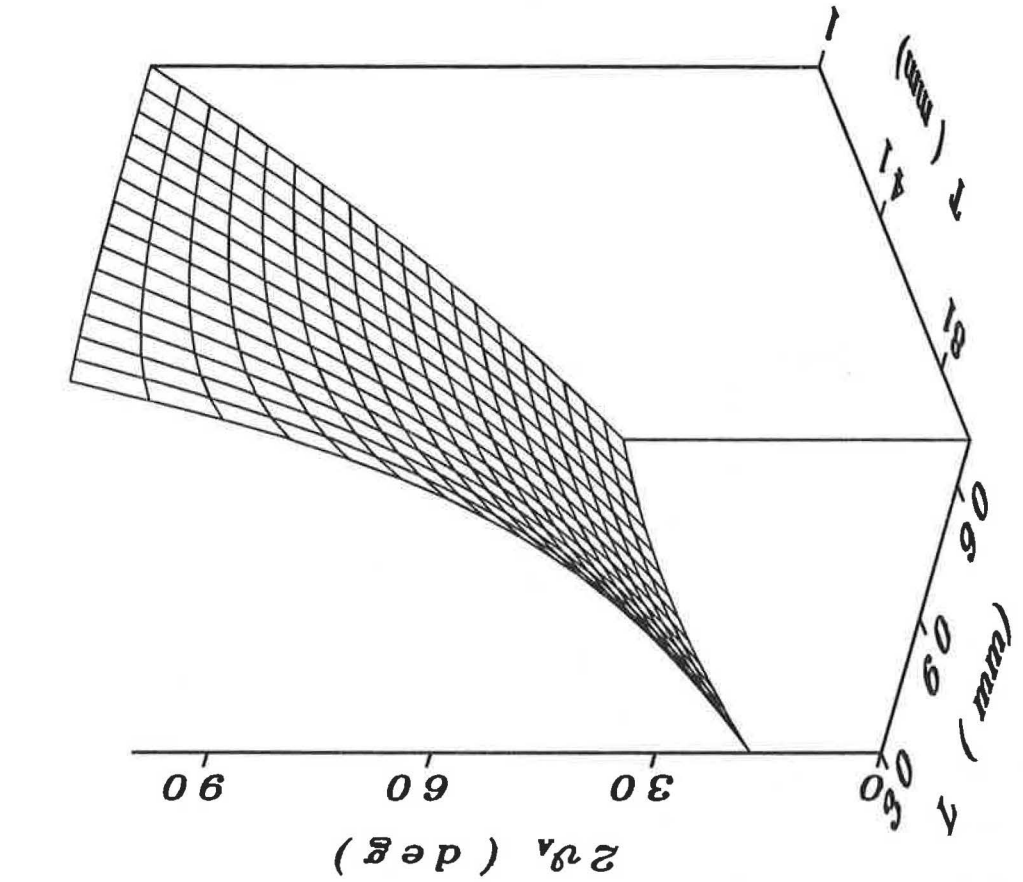
2θA (deg)
0
30
60
90
T (mm)
0
9
18
27
36
r (mm)
1

Fig. 3b

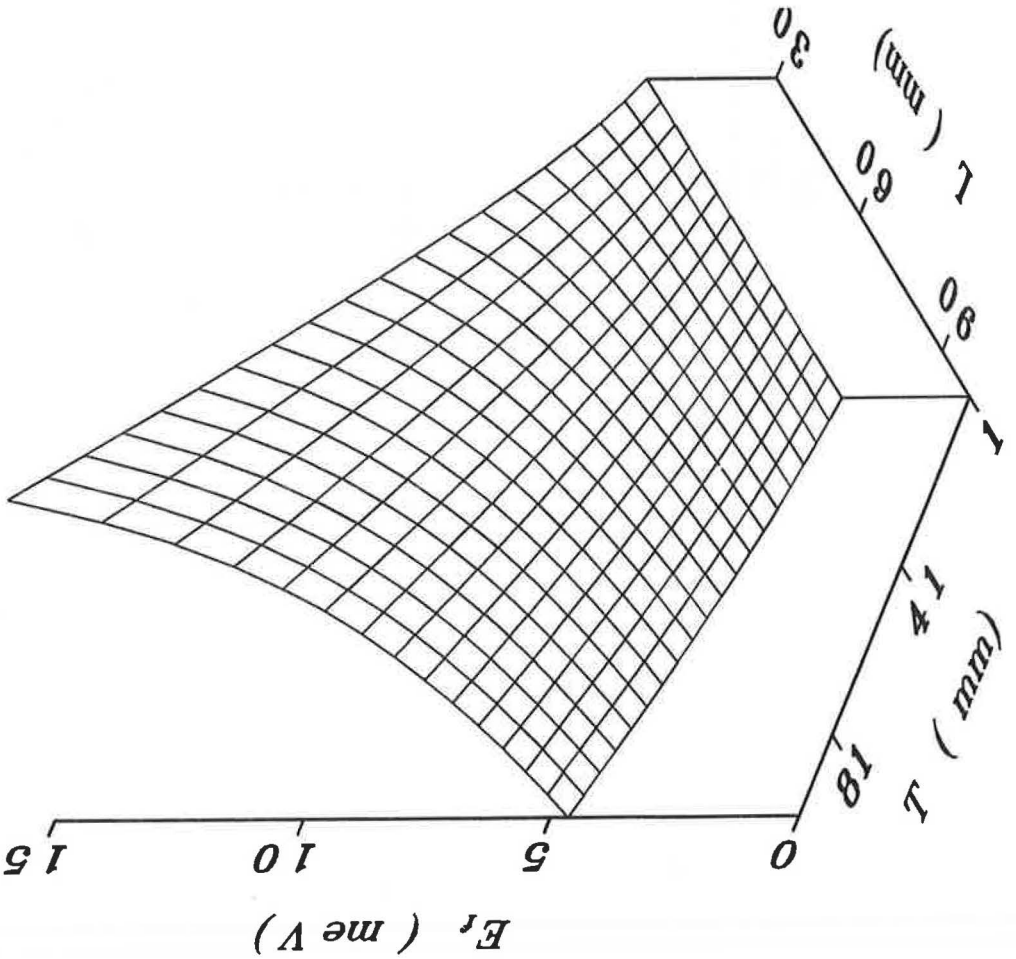
Er (meV)
0
5
10
15
T (mm)
1
4
8
18
r (mm)
1
30
60
90

Fig. 3a

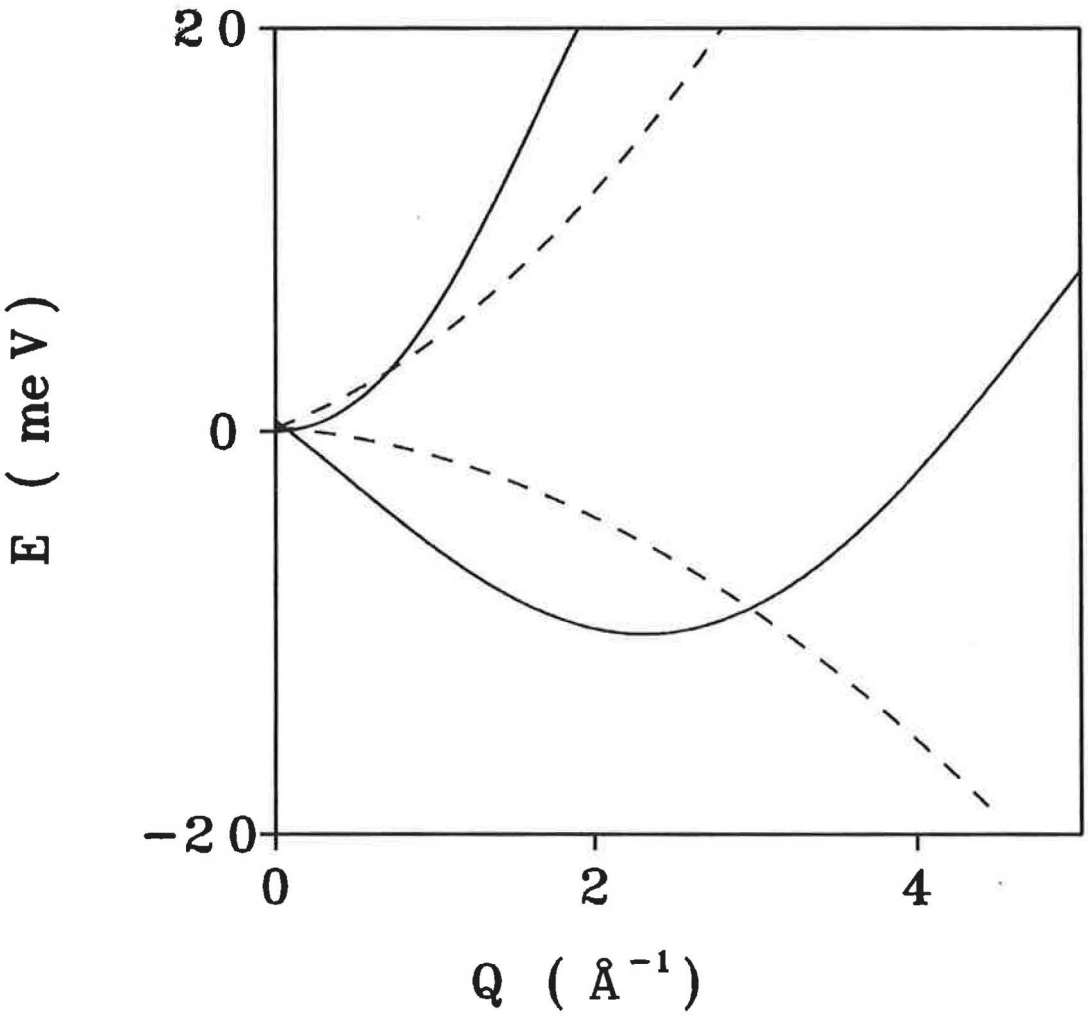

Fig. 4

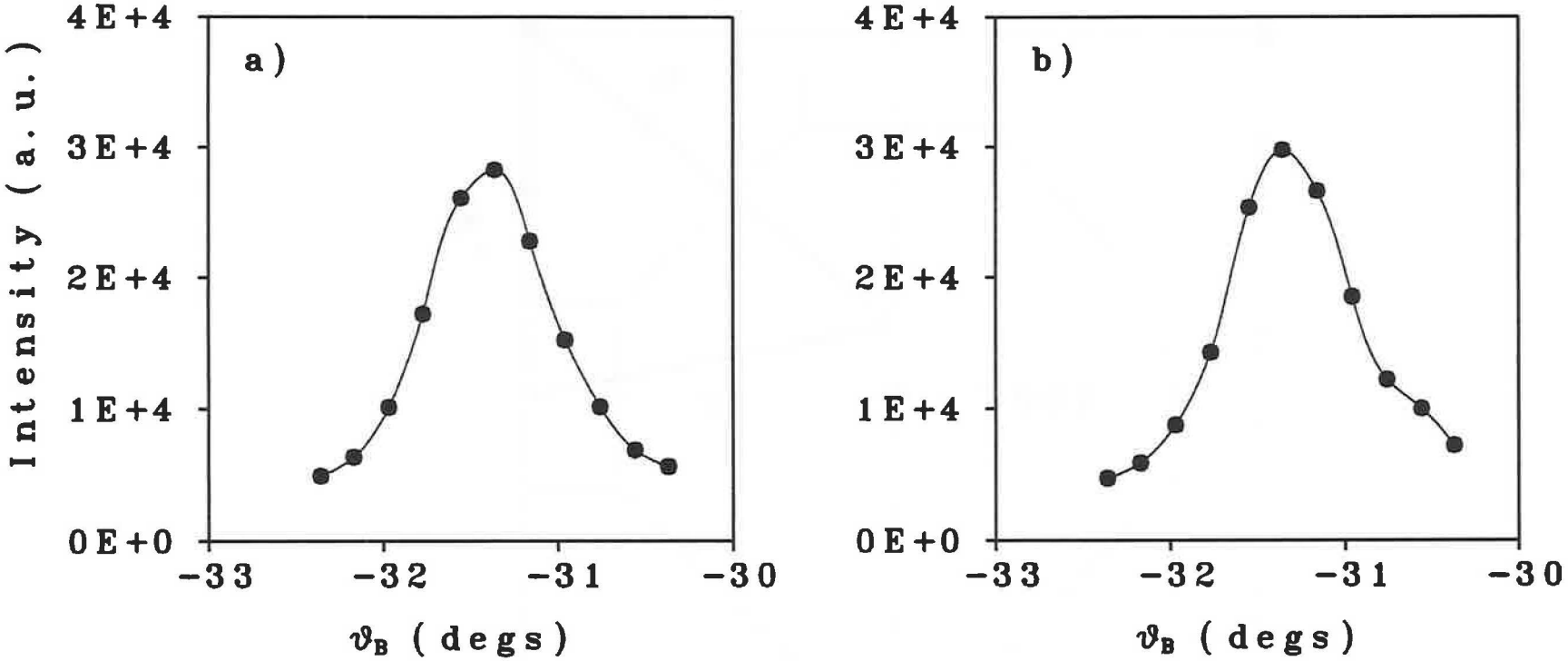

Fig. 5

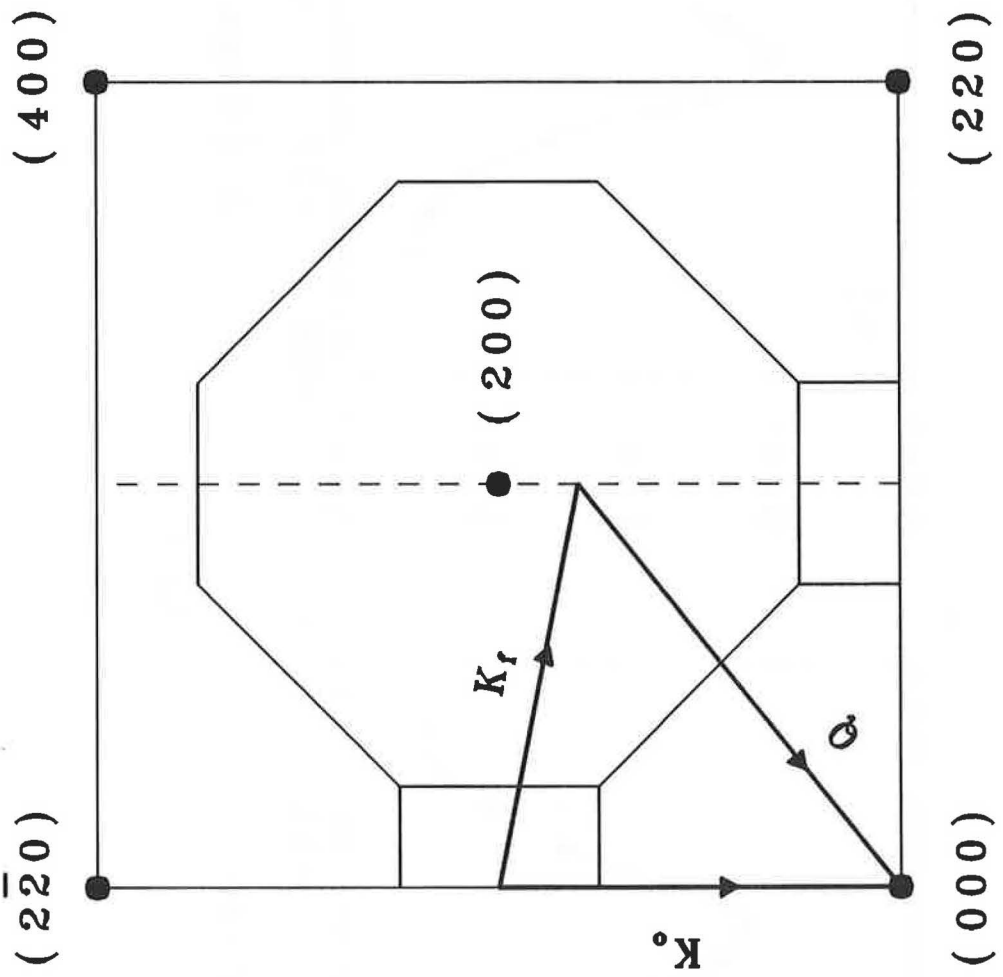

Fig. 6

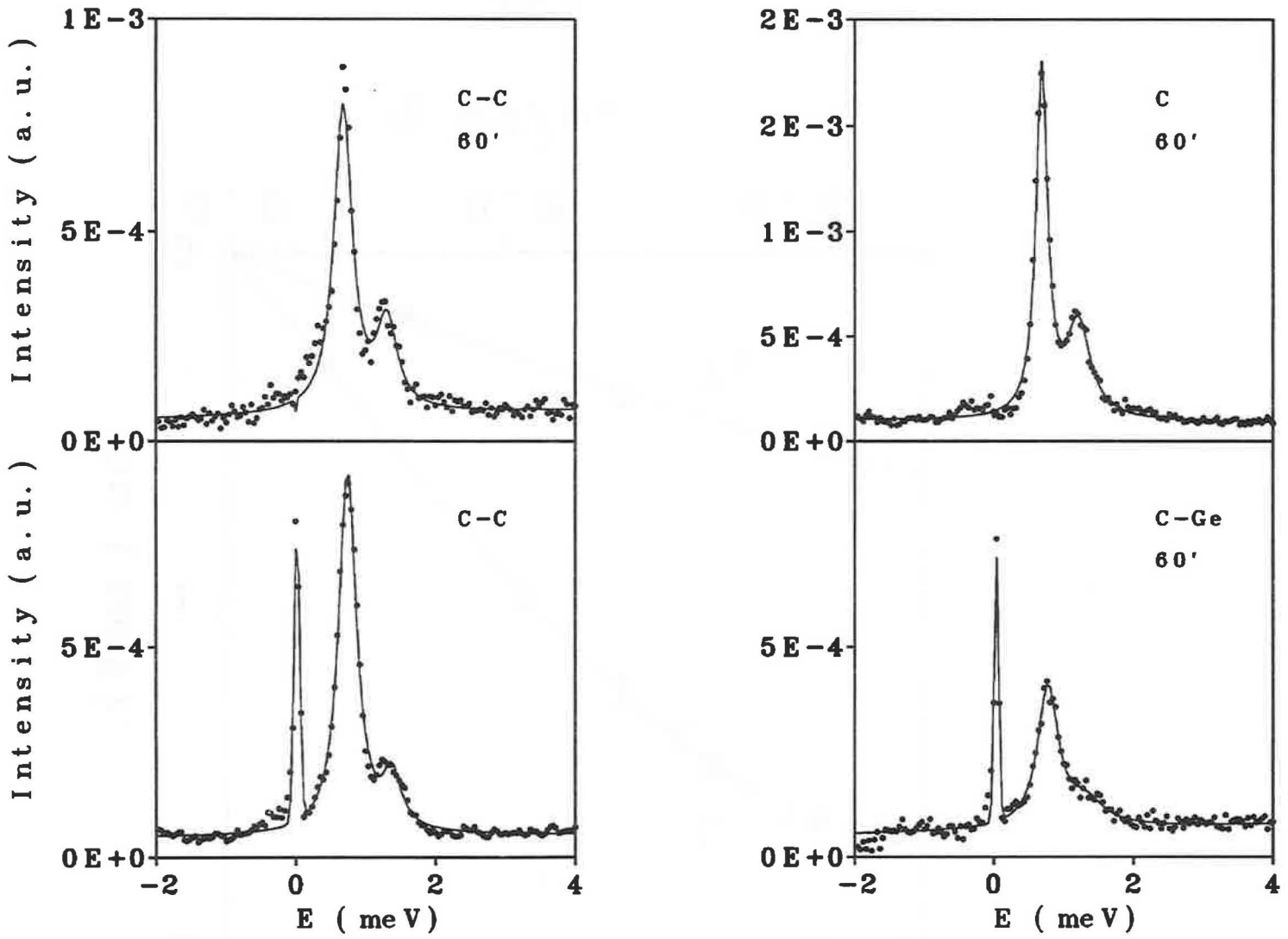
1E-3
5E-4
0E+0
Intensity (a.u.)
C-C
60'
C-C
5E-4
0E+0
Intensity (a.u.)
-2
0
2
4
E (meV)
2E-3
2E-3
1E-3
5E-4
0E+0
C
60'
C-Ge
60'
5E-4
0E+0
-2
0
2
4
E (meV)

Fig. 7

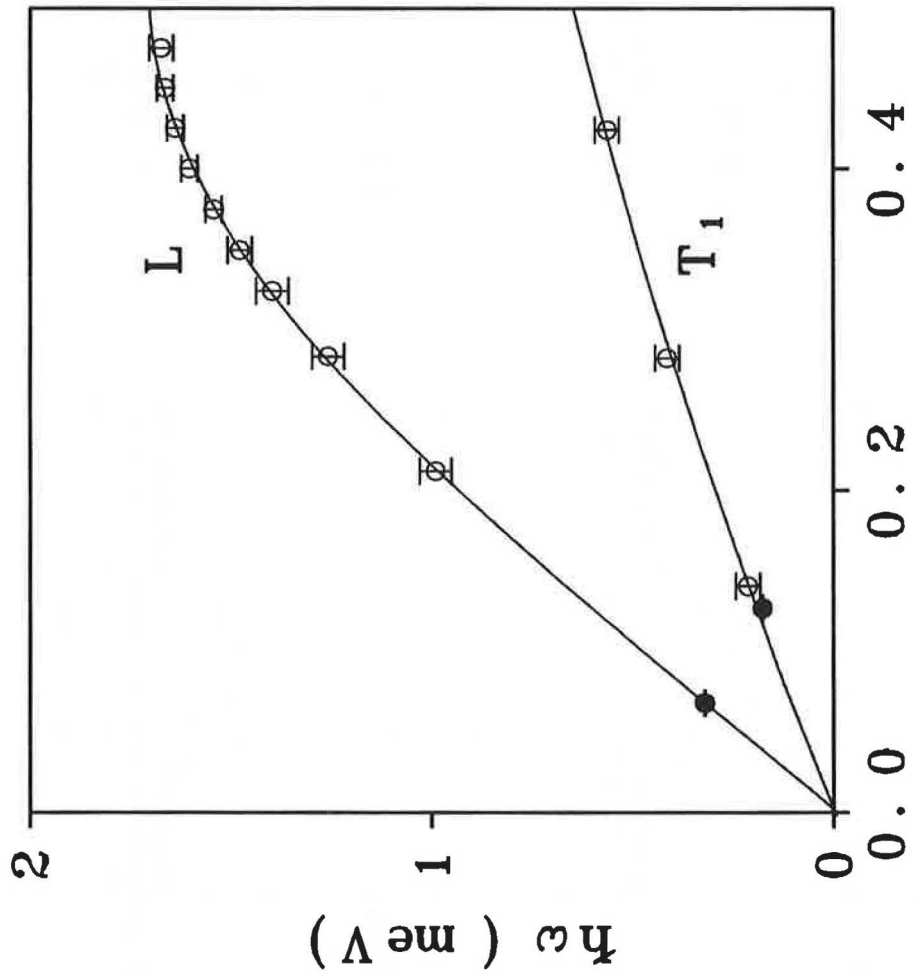

Fig. 8

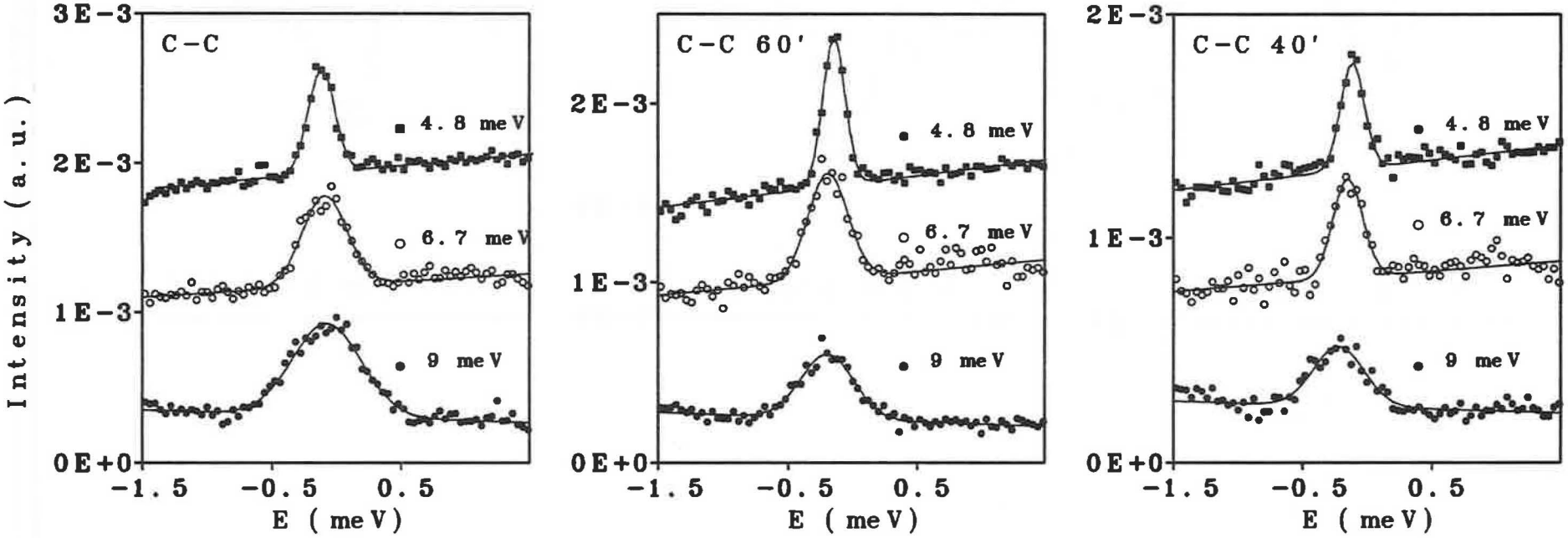
C-C
4.8 meV
6.7 meV
9 meV
3E-3
2E-3
1E-3
0E+0
-1.5
-0.5
0.5
E (meV)
Intensity (a.u.)
C-C 60'
4.8 meV
6.7 meV
9 meV
2E-3
1E-3
0E+0
-1.5
-0.5
0.5
E (meV)
C-C 40'
4.8 meV
6.7 meV
9 meV
2E-3
1E-3
0E+0
-1.5
-0.5
0.5
E (meV)

Fig. 9a

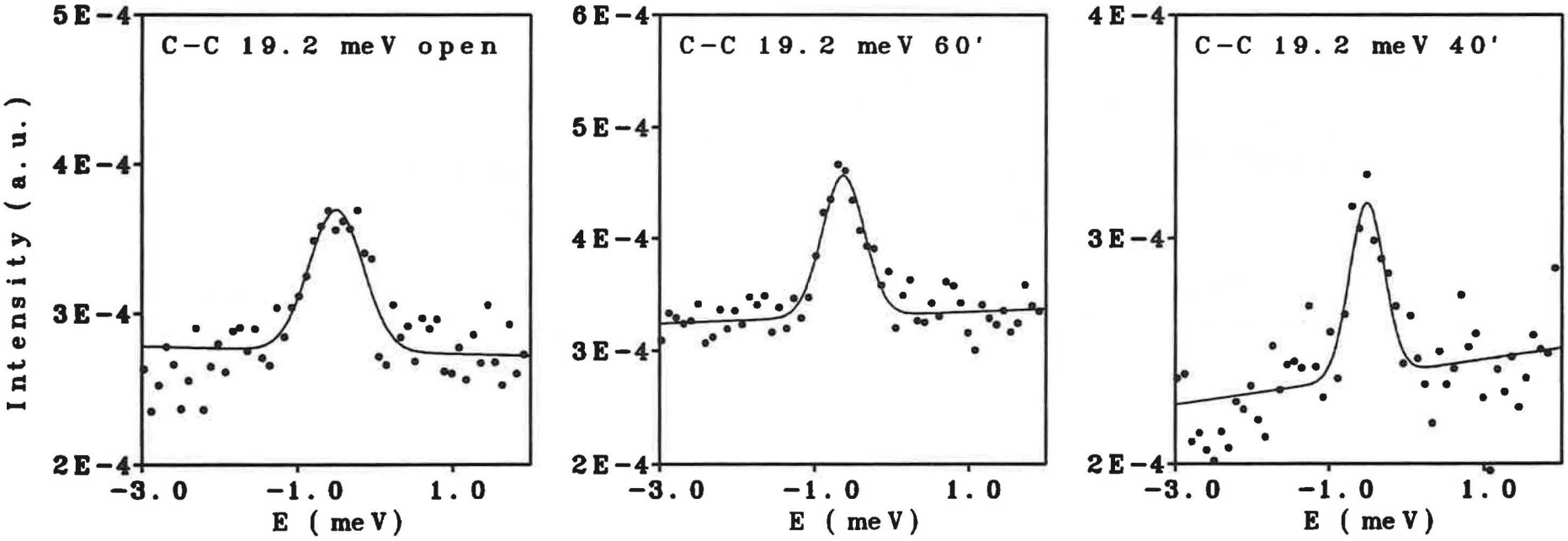
C-C 19.2 meV open
C-C 19.2 meV 60'
C-C 19.2 meV 40'
Intensity (a.u.)
E (meV)
5E-4
4E-4
3E-4
2E-4
6E-4
-3.0
-1.0
1.0

Fig. 9b

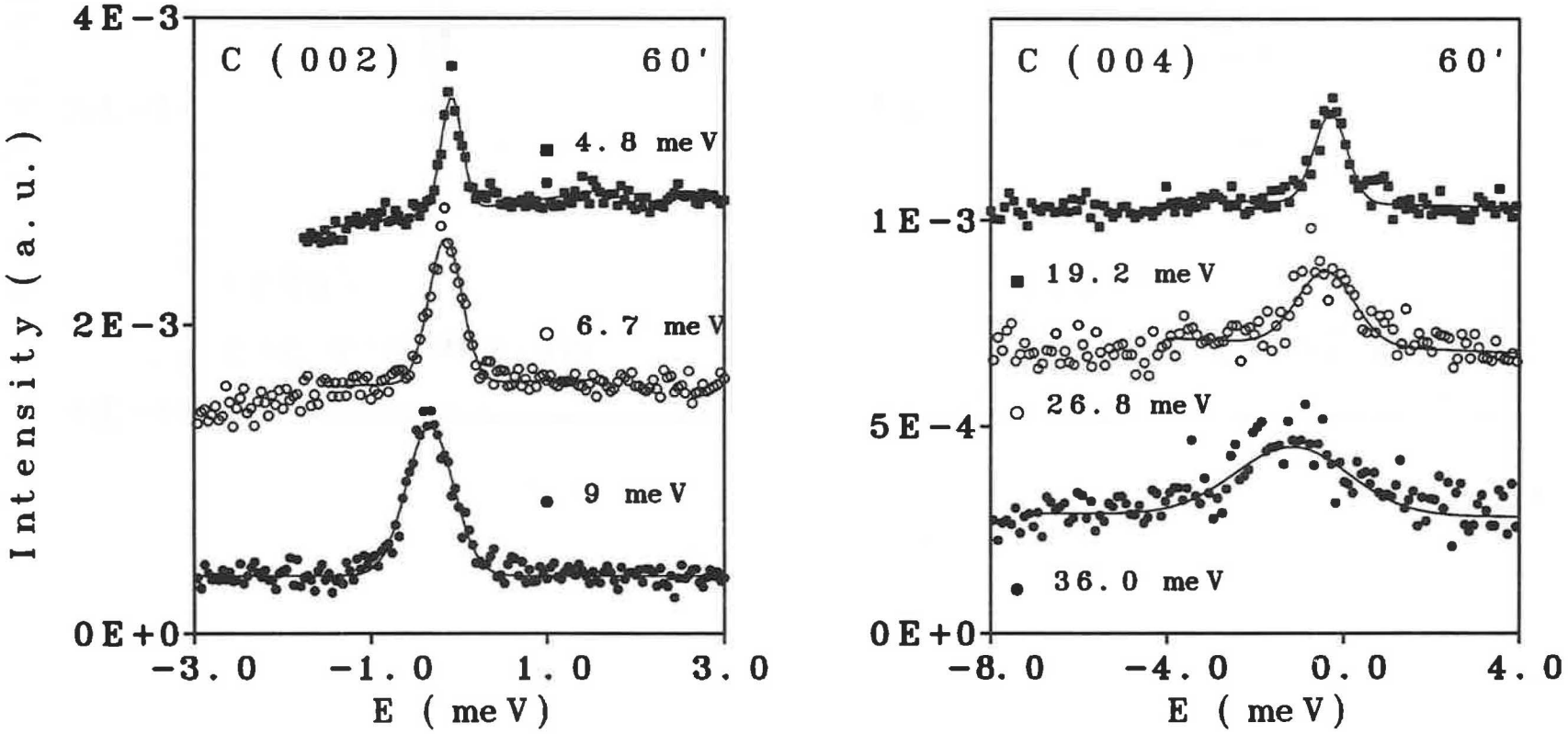
C (002)
60'
4.8 meV
6.7 meV
9 meV
4E-3
2E-3
0E+0
Intensity (a.u.)
-3.0
-1.0
1.0
3.0
E (meV)
C (004)
60'
19.2 meV
26.8 meV
36.0 meV
1E-3
5E-4
0E+0
-8.0
-4.0
0.0
4.0
E (meV)

Fig. 10

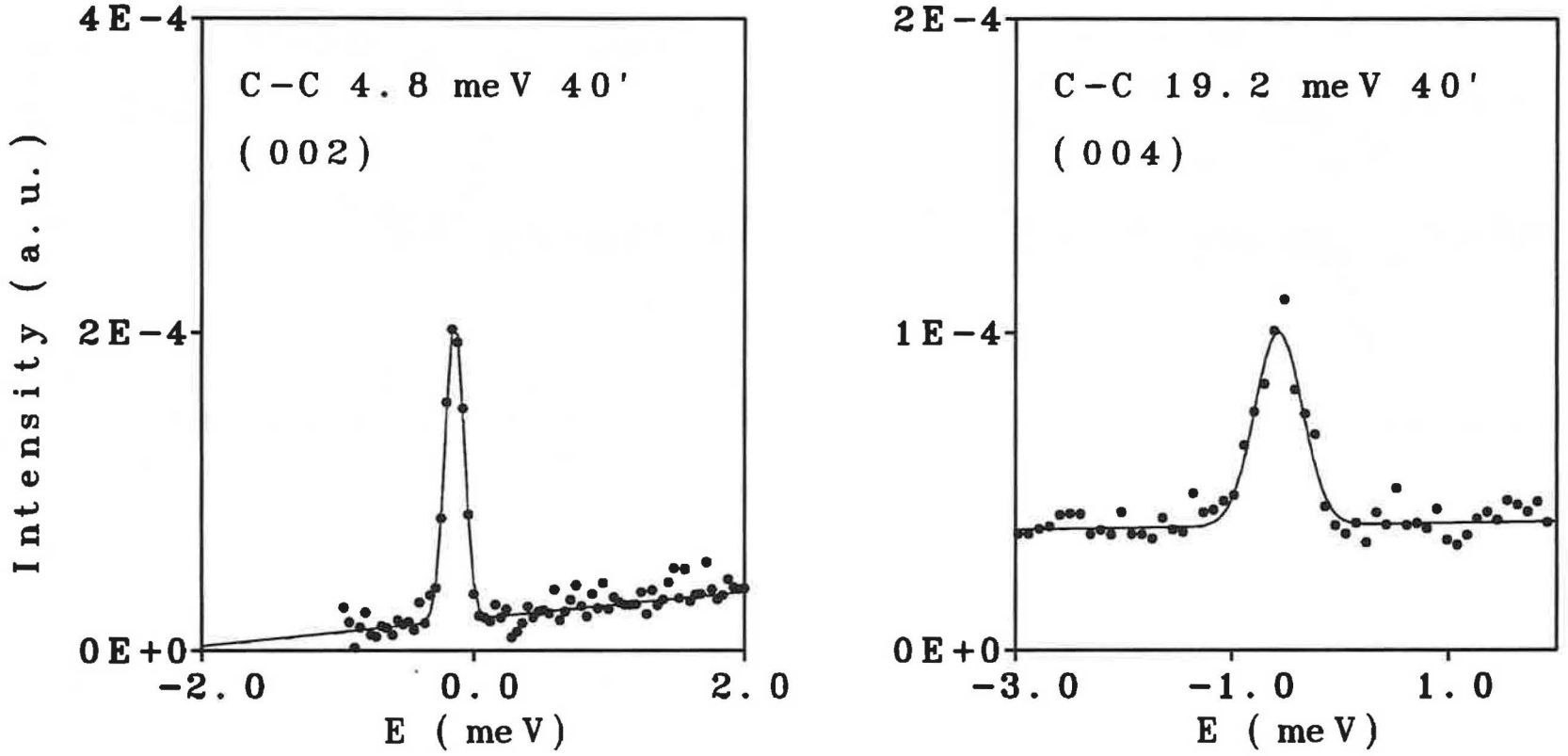
4E-4
2E-4
0E+0
Intensity (a.u.)
C-C 4.8 meV 40'
(002)
-2.0
0.0
2.0
E (meV)
2E-4
1E-4
0E+0
C-C 19.2 meV 40'
(004)
-3.0
-1.0
1.0
E (meV)

Fig. 11

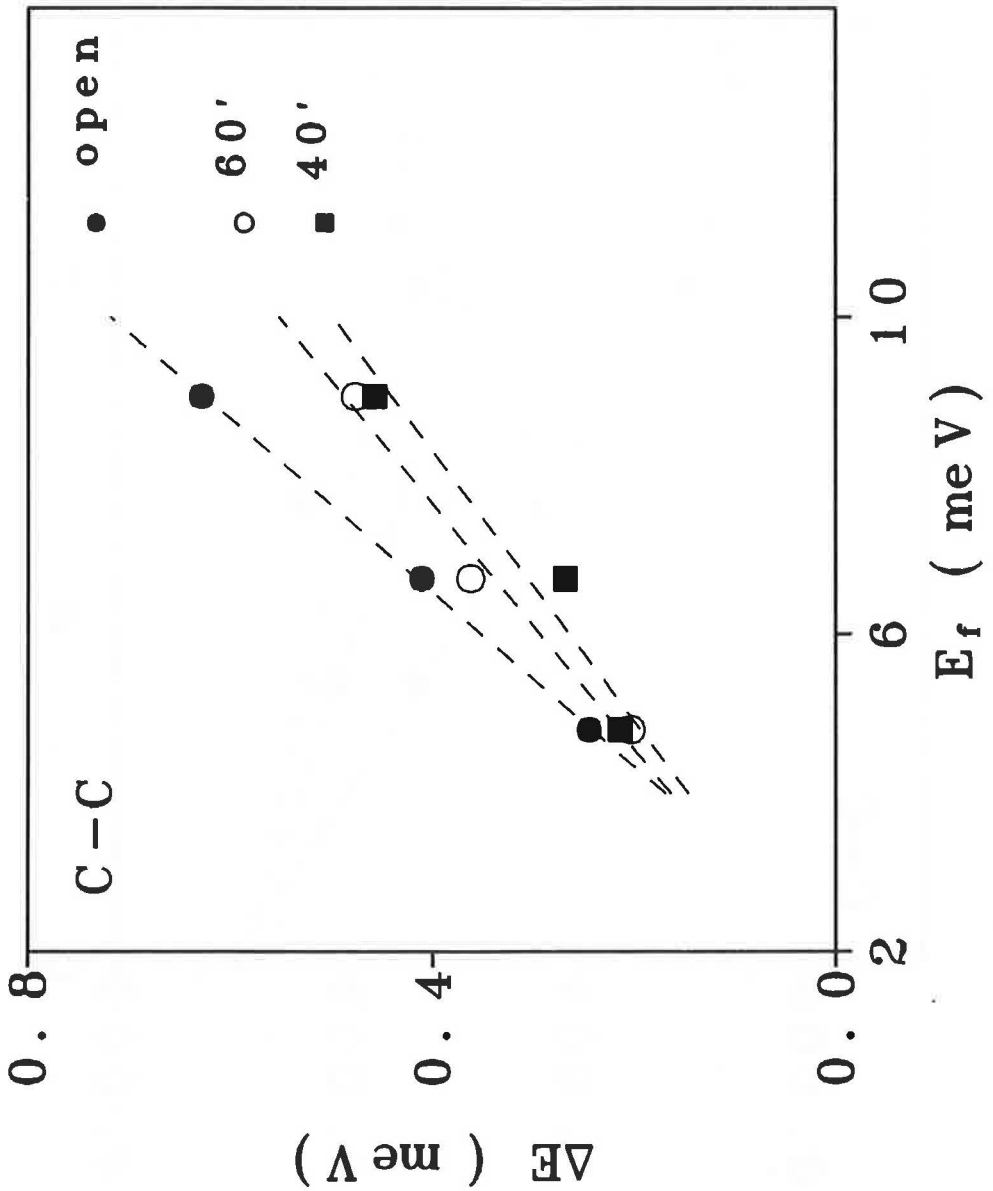

Fig. 12

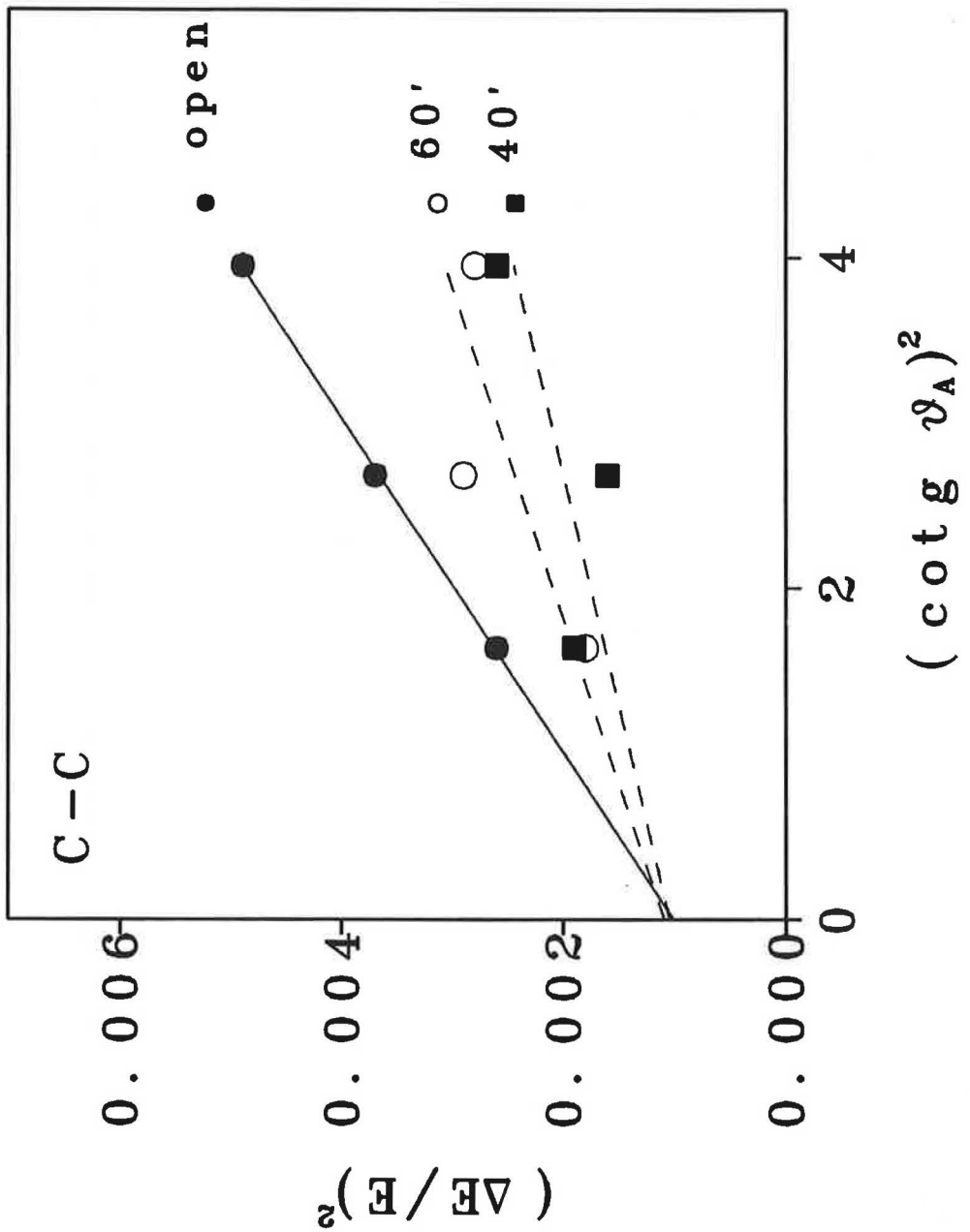
C–C
open
60'
40'
0.006
0.004
0.002
0.000
0
2
4
$(\Delta E/E)^2$
$(\mathrm{cotg}\ \vartheta_A)^2$

Fig. 13